DFT Simulations as Valuable Tool to Support NMR Characterization of Halide Perovskites: the Case of Pure and Mixed Halide Perovskites

Claudio Quarti, Eric Furet, Claudine Katan

DOI: 10.1002/hlca.202000231

FULL PAPER

HELVETICA chimica acta

DFT Simulations as Valuable Tool to Support NMR Characterization of Halide Perovskites: the Case of Pure and Mixed Halide Perovskites

Claudio Quarti,*[a, b] Eric Furet,[a] and Claudine Katan[a]

[a] Univ Rennes, ENSCR, INSA Rennes, CNRS, ISCR (Institut des Sciences Chimiques de Rennes)-UMR 6226 FR-35000 Rennes, France

[b] University of Mons, Laboratory for Chemistry of Novel Materials, BE-7000 Mons, Belgium, e-mail: claudio.quarti@umons.ac.be

For the 75th anniversary of Prof. *Michael Grätzel*

Solid state NMR spectroscopy is swiftly emerging as useful tool to characterize the structure, composition and dynamic properties of lead halide perovskites. On the other hand, interpretation of solid state NMR signatures is often challenging, because of the potential presence of many overlapping signals in small range of chemical shifts, hence complicating the extraction of detailed structural features. Here, we demonstrate the reliability of periodic Density Functional Theory in providing theoretical support for the NMR characterization of halide perovskite compounds, considering nuclei with spin $I = 1/2$. For light ^{1}H and ^{13}C nuclei, we predict NMR chemical shifts in good agreement with experiment, further highlighting the effects of motional narrowing. Accurate prediction of the NMR response of ^{207}Pb nuclei is comparably more challenging, but we successfully reproduce the downshift in frequency when changing the halide composition from pure iodine to pure bromine. Furthermore, we confirm NMR as ideal tool to study mixed halide perovskite compounds, currently at the limelight for tandem solar cells and color-tunable light emission.

Keywords: halide perovskites, NMR spectroscopy, periodic DFT calculations, structure elucidation.

Introduction

Metal halide perovskites are currently under intense scrutiny for opto-electronic applications, in particular photovoltaics and light-emission.[1–3] By combining inexpensive processability from room temperature solution techniques together with excellent semiconducting properties, including large optical absorption coefficient,[4] decent charge mobility[5] and hindered electron-hole recombination,[6] these systems have recently established 25.5% photovoltaic efficiency record,[7] challenging long-time established photovoltaic technologies in the direction for low cost renewable solar energy. This class of materials is characterized by AMX_3 chemical structure, where a continuous network of MX_6 octahedra (M being a divalent metal, Pb, Sn or Ge and X being a halide) in corner shared connection is alternated by a lattice of A-cations, consisting in a small organic molecule ($CH_3NH_3^+$ or $CH(NH_3)_2^+$) and/or an inorganic atomic cation (Cs^+). However, in spite of their impressive opto-electronic performances, our knowledge of the basic properties of these systems remains partly elusive. Halide perovskites are characterized by complex structural properties, as related to the rich chemical tailorability and to the existence of competing allotropic crystalline forms and phase transitions. For instance, the reference methylammonium lead halide ($MAPbX_3$) compounds show two common phase transitions,[8,9] one at low temperature, involving transition from orthorhombic to tetragonal crystal structure, and the other (taking place slightly above

Supporting information for this article is available on the WWW under https://doi.org/10.1002/hlca.202000231

room temperature for the case of $MAPbI_3$) involving a transition from tetragonal to pseudocubic crystal structure. The increased mobility of the A-cation in the high temperature tetragonal and pseudocubic lattices leads to dynamic disorder,[10–14] which impacts the optical and electronic properties of the material.[15] The characterization of this dynamics as function of the composition of the A-site is therefore an important point, to further optimize the performances of perovskite-based devices. Mixed halide perovskites also present several open questions, in terms of their structural characterization. Currently under investigation for wavelength-tunable light-emitting diodes[16] and for tandem solar cells,[17] these materials often show unstable response under operation, because of the formation of halide segregated phases. The possibility to tackle the halide composition and homogeneity from the mesoscale, down to the atomic scale is therefore important for technological applications. Another open question is then related to the so-called hollow[18] and deficient halide perovskites.[19] In these systems, the intentional incorporation of bulky organic cations leads to the formation of defective sites in the lattice. These however do not negatively affect the optical and electronic properties of the material, namely, the optical absorption onset, at least for defect concentration limited to 10%, as reported in Ref.[19] for the specific case of the deficient $MAPbI_3$. Still, quantifying the concentration of defective sites incorporated in the perovskite lattice, establishing whether they are randomly distributed (hollow),[18] or tend to self-organize (deficient)[19] is crucial for the exploitation of this promising class of materials.

In this frame, it clearly appears that in order to achieve a detailed structural characterization of halide perovskites, a smart combination of several techniques is required, so to probe the material structure both on a global scale, as in the case of the XRD, and on a very local scale. Solid state Nuclear Magnetic Resonance (NMR) spectroscopy represents the ideal method for the investigation of the local structure in halide perovskites, as the NMR response of the atoms constituting the material is strongly sensitive to their chemical environment, the nature of the chemical bonds and fine structural details (bond lengths and bond angles). NMR faced an initial success during the 80ies for the characterization of all-inorganic halide perovskite materials, as a complementary technique with respect to XRD. Seminal work by *Roos* and coworkers investigated the phase transition in all-inorganic $CsPbCl_3$ and $RbCdCl_3$ perovskite structures,[20] followed by other NMR-based investigations on the phase transitions of lead halide perovskite systems.[21,22] *Wasylishen et al.* instead performed seminal structural investigations of hybrid methylammonium lead halide perovskite structures by combining NMR measurements with several characterization techniques. Their results nicely highlighted the rotational dynamics associated to the methylammonium cations in the cubo-octahedral cage and further explored the related effects of temperature and phase transitions.[23,24] The interest in the NMR response of metal halide perovskite has rekindled more recently subsequent to their initial breakthrough for photovoltaic (PV) applications in 2012.[25–27] These achievements first prompted additional structural characterization for methylammonium lead iodide perovskite reported by *Baikie et al.*,[28] followed by NMR characterizations of pure bromide and chloride analogues, as well as alloys concomitantly by *Rosales et al.*[29] and *Roiland et al.*[12] These latter studies demonstrated the capability of NMR to characterize phase homogeneity and segregation in mixed halide compounds, through the NMR response of ^{207}Pb nuclei. On the strength of these findings, the last few years witnessed a major increase of the number of NMR studies on halide perovskite materials, both related to structure and composition, as well as, on their structural and compositional evolution upon device operation. Recent studies include the characterization of A-mixed halide perovskites,[30–34] demonstration of halide (iodine) diffusion in working devices,[35] characterization of thermal and water-induced structural decomposition,[36] and characterization of dimensionally confined perovskite systems, as layered 2D systems,[37,38] nanoparticles,[39,40] and deficient-halide perovskites.[19,41] A remarkable overview of results related to NMR characterization of metal halide perovskites can be found in Refs.[42,43].

Meanwhile, despite its successes and possibilities, a detailed interpretation of NMR spectroscopy data is usually a delicate task. Solid state NMR signatures of real samples are not-unfrequently characterized by complex lineshapes, arising from the overlap of several signatures in a small range of chemical shifts and, in the specific case of static measurements, by broadening coming from Chemical Shielding Anisotropy (CSA), hence making reliable assignments challenging. Additional support is therefore greatly welcomed to help the interpretation of experimental data, as nowadays available from periodic Density Functional Theory (DFT) simulations.[44] The development of dedicated approaches from (parameter-free) first-principles theories[44–47] indeed paves the way to provide

complementary information to the experimental NMR characterization, as widely demonstrated in the literature.[48–50] In spite of the number of important studies devoted to halide perovskites, however, the number of DFT simulations targeting NMR parameters is much more scarce. Just in the last years, few NMR investigations included estimates of the magnetic shielding tensor via DFT simulations, mainly exploiting the molecular approach from quantum-chemistry.[31,34,51–54] Here, reliable models for the halide perovskite material are obtained by cutting out a finite cluster.[55] In the present work, we will instead rely on complementary picture from periodic DFT calculations, where a representative crystal cell is replicated in space, a perspective that is more natural to discuss systems in condensed phase. Surprisingly, the periodic approach has been comparably less exploited than the molecular one, for the case of halide perovskites,[12,56] hence leaving a question mark on its reliability and accuracy in predicting the NMR properties of these interesting materials. Here, we perform extensive periodic DFT simulations aimed to unveil advantages and limitations of periodic DFT methods in simulating the NMR response of halide perovskites, with special attention to nuclei with spin quantum number $I = 1/2$, namely ^{1}H and ^{13}C and ^{207}Pb. Simulations will consider reference models for the three phases (orthorhombic, tetragonal and cubic) reported for methylammonium lead iodide and bromide perovskites, hence addressing potential influence of the reference crystallographic model. Finally, we will also simulate the ^{207}Pb response of mixed iodine/bromine compounds, to assess the reliability of DFT simulations in describing these systems, which are attracting large interest for tandem solar cells and tunable-color light emitting devices.[57–60]

Methods

Periodic DFT simulations performed here are based on a series of models for methylammonium lead bromide and lead iodide perovskites, thereafter, named $MAPbBr_3$ and $MAPbI_3$, respectively. Additional models are considered for mixed halide systems, as explained below. Pure halide phases are simulated adopting available reference models from XRD measurements, for the orthorhombic, tetragonal and cubic phases. The model employed to simulate the low temperature orthorhombic phase obeys the Pnma space group symmetry, with its MA cations in antiferroelectric ordering reported in *Figure 1*, as proposed by *Baikie et al.* on the basis of XRD measurements.[61] The tetragonal phase nominally belongs to the I4mcm[62] or I4cm,[9] which results in orientational disorder for the MA cations. For practical calculations, we here consider the specific orientation of the MA cations shown in *Figure 1*. The high temperature pseudocubic phase is instead modeled through $2\times2\times2$ supercell of the nominal Pm-3m crystalline cell. To account for the orientational disorder characteristic of this phase,[13–15,23] we have considered four models, labeled from 1 to 4, with initial random orientation of the MA cations, as shown in *Figure 1*.

NMR response of halide perovskites is computed with periodic DFT simulations, within the plane-wave/pseudopotential formalism, as implemented in the CASTEP suite code.[44,46,63] This makes use of a perturbative approach to compute the chemical shielding tensor of the atomistic model considered. In addition, the present method takes advantage of the GIPAW (Gauge Including Projector Augmented Wave) formalism to reconnect the non-local information from the plane wave basis set to the local information associated to the electron shielding close to the nuclei, meanwhile solving the Gauge problem, typical of finiteness of the basis set.[45,46] Convergence tests have been performed to evaluate the effect of the two main computational parameters, namely, *1*) the kinetic energy cutoff for plane-wave expansion of the electronic wave functions and *2*) the sampling of the first *Brillouin* zone. We anticipate that, although accounting for the contraction of the orbitals due to relativistic effects, the present formalism for the simulation of the shielding tensor does not include Spin-Orbit-Coupling (SOC),[44] which on the other hand turns out to be important for heavy atoms.[55,64–67] Test calculations are performed on the orthorhombic phase of $MAPbBr_3$ (see *Figure 1*), as well as for tetramethylsilane and $Pb(NO_3)_2$, which represent the typical reference compounds for the calculation of NMR chemical shift of ^{13}C and ^{1}H nuclei, and ^{207}Pb, respectively. A 600 eV kinetic energy cutoff and 0.03 $Å^{-1}$ k-point mesh density result in converged values for the magnetic shielding values of ^{13}C nuclei, while providing discrepancy of less than 1 ppm for ^{1}H nuclei, as compared to more expensive computational set-ups (see *Supporting Information*). The chemical shielding of ^{207}Pb shows instead larger deviations, on the order of few tens of ppm (see *Supporting Information*). Still, the larger dependency of this nucleus to the computational approach, as compared to ^{1}H and ^{13}C, should be put in perspective of its very broad range of chemical shifts, on the order of thousands of ppm. Consequently,

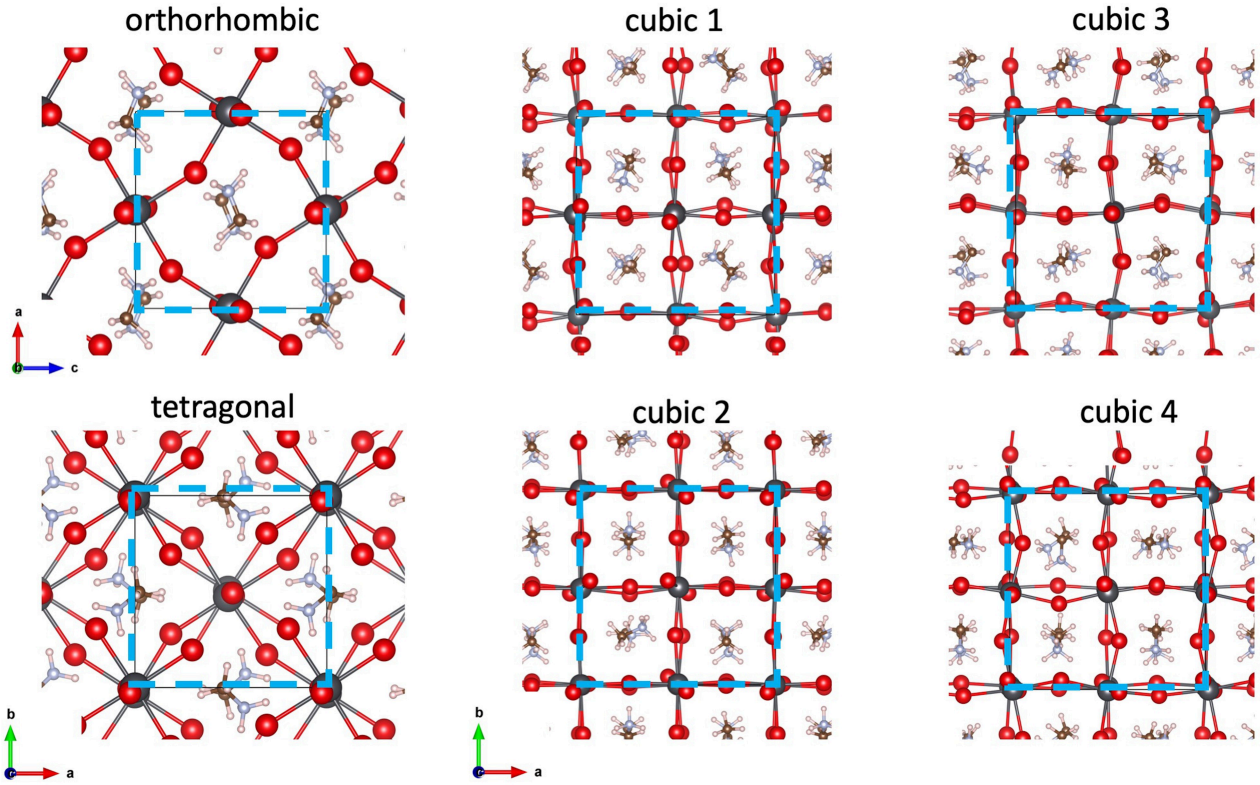

Figure 1. Periodic models adopted for the simulation of the NMR response of $MAPbI_3$ and $MAPbBr_3$ perovskites. Color code is: dark grey = lead, red = halide, brown = carbon, light blue = nitrogen, light pink = hydrogen.

600 eV and 0.03 $Å^{-1}$ were chosen through all this work as the best trade-off between computational cost and accuracy. Unless stated otherwise, all the models in *Figure 1* are optimized with cell parameters kept fixed at their corresponding experimental values. Optimizations were performed adopting the same level of theory used for the calculation of the NMR response (600 eV and 0.03 $Å^{-1}$).

To compare the results from our simulations with experiments, meanwhile addressing the accuracy of our periodic DFT simulations, we resort to widespread and statistically meaningful approach for the appropriate referencing of the computed NMR parameters. This consists in computing theoretical NMR chemical shielding (σ_{iso}) for a set of compounds with known experimental chemical shift (δ_{iso}) and fitting the two datasets with a linear function.[44,47,55,64] The intercept of the line determines the reference for the definition of the chemical shift, while the slope provides indication on the accuracy of the method, with slopes close to −1 corresponding to good quantitative matching between theory and experiment. The results of this procedure for the ^{1}H, ^{13}C and ^{207}Pb nuclei with respect to a set of reference compounds are illustrated in *Figure 2* (details in the chosen datasets are extensively discussed in *Supporting Information*).

Both slope and R^2 coefficient close to −1 for ^{1}H and ^{13}C nuclei, as shown in *Figure 2*, suggest good quantitative accuracy associated to our computational set-up, consistently with previous works adopting the similar periodic DFT approach.[68,69] Results for ^{207}Pb instead suggest lower degree of accuracy for this chemical species, however paralleling previous results reported by *Alkan* and *Dybowski*, adopting non-periodic DFT calculations without accounting for SOC (reported slope of the linear fit and R^2 coefficient are 0.54 and 0.61, respectively).[55] The same authors also demonstrated that inclusion of SOC through Zero-Order Regular Approximation (ZORA) largely improves the results (reported slope and R^2 coefficient of 0.87 and 0.98, respectively),[55] hence demonstrating the necessity of SOC to achieve quantitative accuracy for the prediction of NMR properties of lead-based compounds.

Finally, in the effort of establishing how the detailed atomistic structure influences the predicted

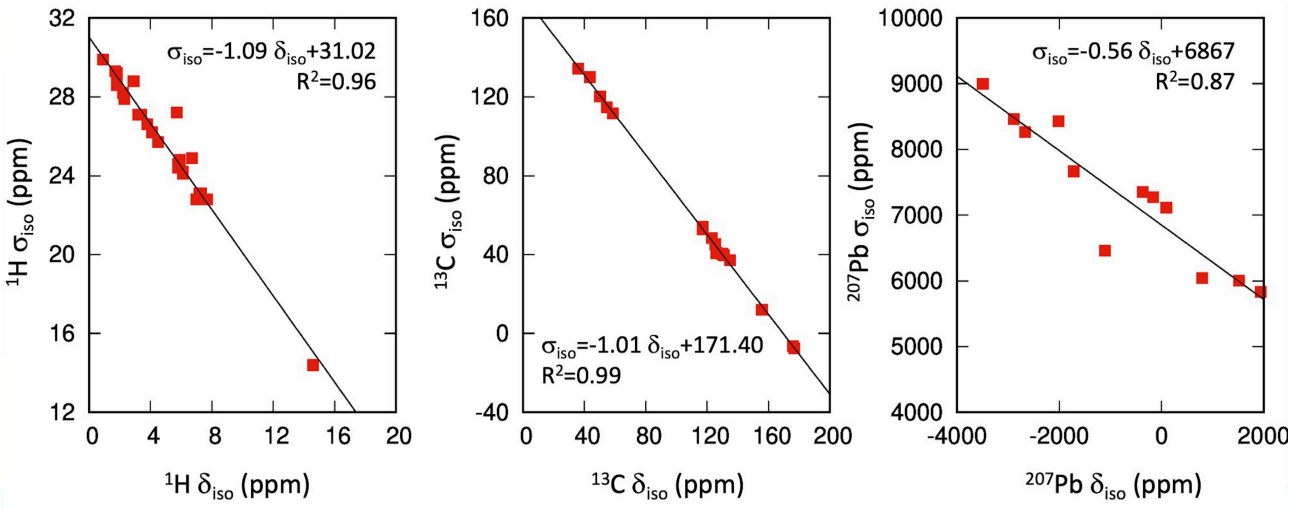

Figure 2. Correlation between experimental chemical shift (δ_{iso}) and computed chemical shielding (σ_{iso}) for ^{1}H, ^{13}C and ^{207}Pb nuclei. Black line represents the best linear fitting to the data, with the corresponding equation and R^2 coefficient reported. Details on the chosen reference compounds and related theoretical parameters are reported in *Supporting Information*.

NMR properties, always within a frozen model picture (as unavoidable for DFT simulations), we performed calculations on differently distorted structures. Similar philosophy was proposed by *Dmitrenko et al.* in Ref.,[66] adopting a molecular description and focusing on the simulation of isolated PbX_6 octahedra (X = halide). Here, we still rely on frozen models of the cubic $MAPbI_3$ model 1, with distorted structures generated from short *Born–Oppenheimer* Molecular Dynamic simulation, hence used here as a simple structure generator, which automatically explores the conformations accessible by the system around the considered equilibrium structure, at a given temperature. This simulation was also performed with CASTEP, with the same computational parameters as for the previous calculations. 10 ps trajectory were generated, with time step of 1 fs, and employing an NVT ensemble, with target temperature fixed at 300 K, using *Nose-Hoover* thermostat.[70] Consistently, a set of 50 snapshots have been extracted each 200 fs for additional NMR simulations, as we will discuss later.

The spectra have been simulated from the NMR chemical shielding tensors computed from DFT, adopting the SIMPSON program.[71] In fact, SIMPSON is known to incorporate some aspects of the experimental spectral acquisition process. However, it does not consider the effects of rapid longitudinal (T1) relaxation of halide/halide chemical exchange nor homogeneous ^{207}Pb transverse (T2) relaxation.[72–74] Second, limited excitations brought about by the finite RF pulses used for excitation and the limited receiving bandwidth of the probe may cause intensity deviations. Additionally, our simulations do not account for scalar/dipolar couplings to halogens and the effects of halogen nuclei spin relaxation on the ^{207}Pb-NMR spectra.

Results

NMR Signals from Light ^{13}C and ^{1}H Nuclei

NMR spectroscopy of ^{13}C is informative of the organic chemical species incorporated into the perovskite and has been thoroughly exploited for hybrid halide perovskites, as consequence of the continuous increase in the complexity of their chemical formulation. For instance, it has been used for characterizing mixed A-cation methylammonium/formamidinium compounds,[30,75] to unveil structural details related to the organic spacer in layered 2D halide perovskites,[76] and to determine the successful incorporation of hydroxy-ethylammonium in deficient perovskites.[19] NMR Spectra of light ^{13}C nuclei as computed from DFT calculations for the various perovskite structural models for $MAPbBr_3$ and $MAPbI_3$ are shown in *Figure 3*, in comparison with experimental data. Translation of the computed chemical shielding in chemical shift directly follows the results from *Figure 2*. Experimental data in *Figure 3,a* are obtained from Magic Angle Spinning (MAS) NMR measurements from Ref.,[19] performed at room temperature. Theoretical chemical shifts are spread between 23 ppm and 31 ppm, as function of

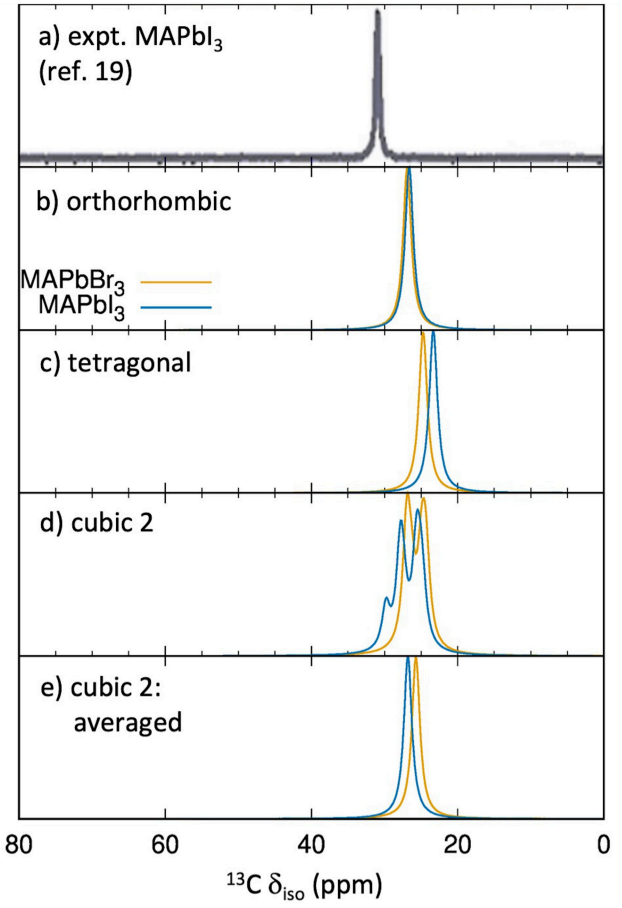

Figure 3. Magic Angle Spinning (MAS) NMR spectrum of ^{13}C nuclei of $MAPbI_3$ from experiment (a) and DFT calculations (b–e) for pure halide perovskites. (a) MAS NMR measurement of $MAPbI_3$ from Ref.,[19] as measured at room temperature; (b–d) computed MAS NMR spectrum for the $MAPbBr_3$ (orange line) and $MAPbI_3$ (blue line) on the orthorhombic (b), tetragonal (c) and on cubic 2 (d) models (see *Figure 1*); (e) MAS NMR obtained for model cubic 2, by averaging over the different carbons constituting the model, to account to some extent for motional narrowing (see text). Experimental data in *Figure 3,a* adapted with permission from Ref.[19] ©2017 *Wiley-VCH*.

the specific model considered, and are hence slightly underestimated with respect to the experimental results but still in overall nice agreement. The difference between NMR signals for $MAPbBr_3$ and $MAPbI_3$ depends also on the structural model considered and is overall small, hence indicating limited influence of the halide on the NMR response for ^{13}C. This finding is consistent with other experimental evidence from the literature.[28] NMR lineshapes computed for the orthorhombic and tetragonal phases are consistent with only one signal, with the former in nice agreement with respect to MAS NMR measurement performed in Ref.[30] at 100 K, that is, within the stability range of the orthorhombic phase. The lack of dispersion in the NMR response from the four carbon atoms composing the orthorhombic (tetragonal) model should be traced back to the fact that these atoms are equivalent (quasi-equivalent) because of the space group symmetry of this system. In other words, because of the crystal symmetry, the MA cations experience the same chemical environment (computed isotropic shielding are reported in *Supporting Information*, for the sake of completeness). Frozen cubic models of $MAPbI_3$ and $MAPbBr_3$ instead are characterized by broader NMR signals. This is illustrated in *Figure 3,d* for the special case of the model cubic 2 (*Figure 1*), that is found to be the most stable among the four proposed cubic models, for which we computed NMR chemical shifts ranging from 24 ppm to 30 ppm. However, similar broadening can be noticed for all considered cubic models (see *Supporting Information*). In contrast to the orthorhombic phase, C-atoms in the cubic models in *Figure 1* are symmetry-inequivalent, hence feeling slightly different chemical environments which, in turn, results in NMR chemical shifts dispersed within a few ppm (*Figure 3,d*). The broadening of the spectrum is therefore informative about the local environment differences, at least in principle. On the other hand, this broadening is not found experimentally at room temperature (see *Figure 3,a*),[19,28] because of the occurrence of motional narrowing, that is, a decrease of linewidth when increasing the temperature. This phenomenon is characteristic of NMR techniques and is due to the fact that the correlation time for MA cation dynamics, lying in the pico-second time-scale,[15,23] is much shorter than the typical time-scale probed by NMR.[50,77] As a result, because of the dynamic disorder associated to the thermal re-orientation of the MA cations at finite temperature, the NMR will not result from the convolution of the individual conformations or orientations but to an average response. A striking example from literature is represented by the ^{17}O-NMR signals in hydrous magnesium silicates systems.[78] These systems are characterized by rapid proton transfer between different crystalline sites and *Griffin et al.* hence simulated the corresponding ^{17}O-NMR response by averaging out the signals from oxygen atoms in symmetry equivalent sites. Theoretical spectra obtained following this procedure were in much better agreement with respect to the experiment, compared to the non-averaged spectra resulting from the convolution of the various oxygen species. Motional narrowing for the high temperature cubic phase of $MAPbBr_3$ and $MAPbI_3$ was modelled here following a similar procedure. The resulting

spectrum is shown in *Figure 3,e* and recovers similar agreement as the low temperature orthorhombic (*Figure 3,b*) and tetragonal (*Figure 3,c*) phases, further demonstrating importance of dynamic disorder at ambient conditions. We recall however that the reduced broadening of NMR signatures in the low and high temperature phase, as evidenced from MAS measurements in Ref.[30] and,[19] respectively, should be associated to two different mechanisms. For the low temperature phase, this corresponds to very similar chemical environment experienced by the MA cations, as due to crystal symmetry, while in the high temperature phase, this should be rather associated to motional narrowing.

NMR Spectra of ^{1}H nuclei computed for $MAPbBr_3$ and $MAPbI_3$ perovskites are shown in *Figure 4*, compared to experimental results. Also, in this case, definition of the chemical shift from the computed shielding comes from the result in *Figure 2*. Experimental data are obtained from MAS NMR measurements performed at room temperature, from Ref.[12] and show the presence of two signals close to 4 and 7 ppm, associated to hydrogens of the methyl and ammonium groups, respectively. Corresponding theoretical data in *Figure 4,b–4,d* account for the motional narrowing through averaging over the chemically equivalent hydrogen atoms residing on the CH_3 and NH_3^+ groups of the MA cation (see above) and result in predicted chemical shifts at 4 ppm and 8 ppm. Hence, DFT reproduces the experimental data with reasonable accuracy and is consistent with the assignment proposed in the literature. Again, the difference between the ^{1}H isotropic shifts computed for $MAPbI_3$ and $MAPbBr_3$ is small and comparable to the error associated to the computational parameters. We therefore conclude that the halide has limited influence on the NMR response of ^{1}H nuclei, as found experimentally in *Figure 4,a*.

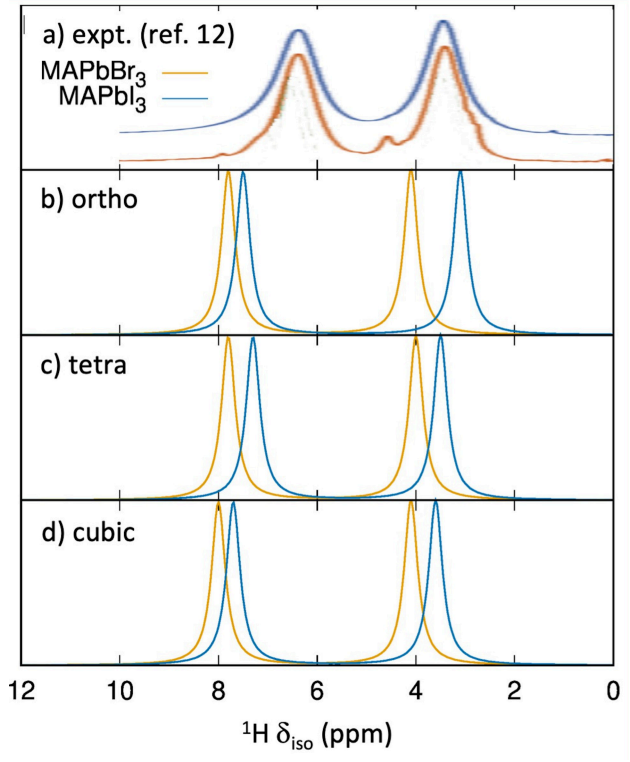

Figure 4. Magic Angle Spinning (MAS) NMR spectrum of ^{1}H nuclei from room temperature experiment (a) and DFT calculations (b–d) for pure halide $MAPbBr_3$ (orange line) and $MAPbI_3$ (blue line) perovskites. (a) MAS NMR measurement, as measured at room temperature; (b–d) computed MAS NMR spectrum for the $MAPbBr_3$ (orange line) and $MAPbI_3$ (blue line) on the orthorhombic (b), tetragonal (c) and on the cubic 2 (d) model. Signals from hydrogens belonging to the CH_3 and NH_3^+ groups are averaged, to account to some extent for motional narrowing (*vide supra*). Experimental data in *Figure 4,a* adapted with permission from Ref.[12] ©2016 *Royal Society of Chemistry*.

NMR Signals from ^{207}Pb in Pure and Mixed Halide Perovskites

Signals from ^{207}Pb and from the halide can instead provide a direct insight into the structural and dynamic properties of the inorganic lattice, which is responsible for the main electronic properties of this class of semiconductors.[79,80] On the halogen side, both ^{127}I and ^{79}Br represent abundant isotopes that can be probed by NMR. However, these two halides possess spin quantum number larger than 1/2, hence featuring significant quadrupolar moments, which in turn makes the measurement of their NMR of the more challenging.[81] NMR measurements of the halide species composing all inorganic $CsPbX_3$ perovskites have been reported in the literature only very recently.[39,42] In turn, ^{207}Pb nuclei are widely investigated through NMR spectroscopy, although the associated broad signatures sometimes make difficult to derive detailed structural features from NMR spectroscopic measurements.[66,67,82] Static NMR measurements are reported in *Figure 5,a*, for pure halide $MAPbI_3$, $MAPbBr_3$ and $MAPbCl_3$ perovskites, as performed at room temperature.[12] Chemical shifts from ^{207}Pb nuclei indeed cover a range of around 2000 ppm, from $MAPbCl_3$, peaked at −644 ppm, to $MAPbI_3$, peaked at 1430 ppm. Furthermore, *Figure 5,a* clearly highlights the sensitivity of the ^{207}Pb signal to the halide composing the perovskite.

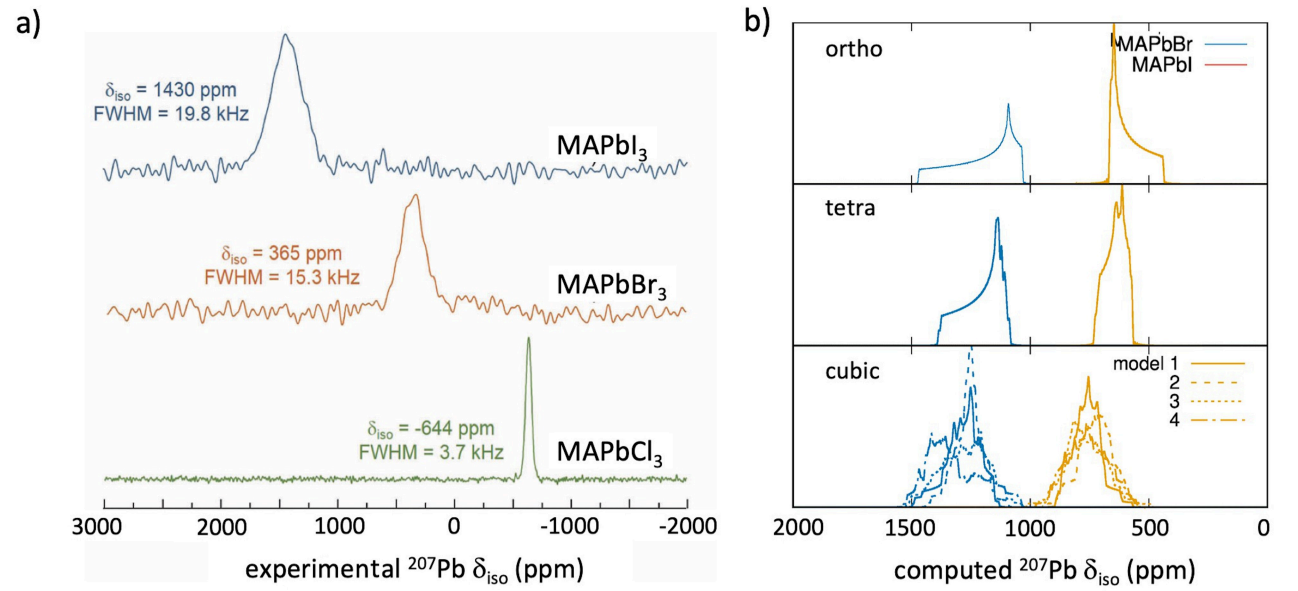

Figure 5. (a) Experimental static NMR spectrum of pure halide $MAPbI_3$, $MAPbBr_3$ and $MAPbCl_3$ perovskites, as measured at room temperature and referenced to $Pb(NO_3)_2$; (b) Static NMR spectrum computed through DFT calculations, performed on the orthorhombic, tetragonal and cubic models of $MAPbI_3$ and $MAPbBr_3$. *Figure 5,a* reproduced with permission from Ref.[12] ©2016 *Royal Society of Chemistry*.

Results from our calculations performed on the orthorhombic, tetragonal and cubic structures of $MAPbBr_3$ and $MAPbI_3$ are given in *Figure 5,b*. The isotropic shift computed for $MAPbBr_3$ sets between 585 and 838 ppm, nicely matching the experimental datum in *Figure 5,a*, while that of $MAPbI_3$, which lies between 1194 and 1460 ppm, is slightly underestimated, consistently with the $|\text{slope}| < 1$ in *Figure 2* (computed NMR parameters are reported in *Supporting Information*). The discrepancy between experimental and DFT chemical shifts cannot be associated to non-converged or inaccurate computational protocol, as preliminary convergence tests clearly showed minor influence (*ca.* 30 ppm) of plane-wave cutoff and sampling of the first *Brillouin* zone, on the predicted NMR response of ^{207}Pb nuclei (see *Supporting Information*). In addition, the systematic error found for the different structural models discourages the assignment of the theoretical-experimental discrepancy to a supposed poor quality of the structural models employed here. Therefore, we believe that the main limitation of the present computational protocol is due to the lack of SOC. Many theoretical calculations from the literature indeed highlighted sizable contributions of SOC on the NMR response of heavy atoms, on the order of 1000 ppm for ^{119}Sn[83] and ^{125}Te,[64] and of 3000 ppm for ^{207}Pb,[65–67] hence providing at least a crude correction for the effect of SOC on the chemical shielding of ^{207}Pb. Most notably, by employing non-periodic calculations accounting for SOC through ZORA, *Alkan* and *Dybowski* obtained estimated isotropic shifts for a set of lead-based compounds which correlated very well with the corresponding experimental data (slope for the linear fitting was 0.87, to compare to our value of 0.56 as reported in *Figure 2,c*. The latter, in turn, is very close to the value of 0.54 that these authors obtained without SOC).[55]

Apart from the absolute value of the chemical shift of ^{207}Pb computed for $MAPbI_3$ and $MAPbBr_3$ perovskites, the present DFT calculations predict the chemical shift of ^{207}Pb with correct order with respect to halide composition, with reported downshift from pure $MAPbI_3$ to pure $MAPbBr_3$ of ~700 ppm, against ~1000 ppm found experimentally (see *Figure 5*). This result is indeed very important, as it provides theoretical confirmation of the experimental findings and paves the way for the theoretical support to NMR characterization of lead perovskites with mixed halide composition. This is currently a hot topic in the literature, with preparation of stable mixed halide systems at the limelight for color-tunable light emission applications and tandem solar cells.[57–60] The lineshape for the tetragonal and orthorhombic phases is strongly asymmetric and does not match the experimental signal. This result consistent with just

one single signal is not surprising and is due to symmetry equivalency among the four lead atoms in the unit cell, further characterized by large CSA, on the order of 400 ppm. Static NMR spectrum computed for the four frozen-cubic models in *Figure 1* instead are characterized by more symmetric shapes of the spectra, arising from the convolution of eight symmetry inequivalent lead atoms in the cell. Notably, the lineshapes computed for these models are in far better agreement with respect to the experimental data, compared to those obtained on the orthorhombic and tetragonal models and could lead to the conclusion that the broad lineshapes of ^{207}Pb nuclei in $MAPbX_3$ perovskites may be related to a distribution of signals. However, previous works discourage this interpretation. Namely, *Rosales et al.* addressed the broadening observed in static NMR experiments (as those in *Figure 5,a*) to homogeneous broadening,[29] while *Aebli et al.* found sizable dipolar coupling between the lead atom and the surrounding halides, as evidenced from MAS NMR measurements, at least on the cesium-based, chlorine and bromine-based lead compounds.[82] In this frame, it is worth to recall that the theoretical simulations in *Figure 5,b*, whose lineshape is dictated both by different values of the isotropic shifts and by CSA, must be addressed to the use of frozen-models, that does not consider for the rapid re-orientation of the MA cation.

In light of the success of DFT simulations in reproducing qualitatively the relative chemical shift of ^{207}Pb nuclei as function of the halide composition of the perovskite, we further tested the capability of this approach to provide information on mixed halide perovskites. Halide mixing represents in fact an effective strategy to tune the optical properties of halide perovskites, for instance in relation to the wavelength of light emission,[57,58] and to improve the performance and stability of related opto-electronic devices.[59] Experimental NMR spectrum of mixed halide perovskite with nominal composition $MAPbIBr_2$ is depicted in *Figure 6,a*, in comparison to the spectra of pure phase iodine and bromine analogues. The mixed halide compound shows two main ^{207}Pb peaks, the first at intermediate frequency with respect to $MAPbI_3$, and $MAPbBr_3$ and the second in correspondence to pure bromine composition component, assigned to mixed halide phase and segregated bromine-rich phase, respectively.[12] At the same time of the result by *Roiland et al.* in *Figure 6,a*,[12] *Rosales et al.* investigated similar mixed halide I:Br systems, similarly demonstrating how ^{207}Pb-NMR response is informative of the presence of halide segregated phases and solid state halide solutions, and how synthetic approach may affect the halide distribution in the material.[29] Subsequently, two independent works by *Hanrahan et al.*[73] and *Karmakar et al.*,[56] investigated mixed Cl:Br halide perovskites, both nicely evidencing the different chemical response of the ^{207}Pb nuclei, as function of the surrounding halide species.

Mixed halide perovskite models are derived here from the cubic 2×2×2 supercell model from *Figure 1*, in light of the more realistic NMR response, compared to experiment. Mixed halide models have been prepared considering I:Br ratio and halide segregation. I:Br compositions correspond to 75:25 50:50 and 25:75 (nominal compositions $MAPbI_{2.25}Br_{0.75}$, $MAPbI_{1.5}Br_{1.5}$, $MAPbI_{0.75}Br_{2.25}$). In relation to halide segregation, we considered four 2×2×2 models for each composition, numbered as alloy1-alloy4, going from situation where the different halide segregated in different PbX_6 octahedra (alloy1) towards more homogeneous situations, that is, where the composition of all the PbX_6 octahedra reflects the nominal composition. A more detailed analysis of the composition of these models is reported in *Supporting Information*. Static NMR spectra as computed from DFT simulations for all mixed halide chemical compositions and considering more (alloy1) or less halide segregated (alloy4) models are reported in *Figure 6,b*. Mixed halide phases show progressive global shift of the ^{207}Pb-NMR signal toward lower frequency, with increasing bromine content, hence in line with the experimental result in *Figure 6,a*. Furthermore, mixed halide models are characterized by more dispersed ^{207}Pb-NMR signal, as compared to pure phase models. This is easily correlated to the contributions from PbX_6 octahedra characterized by different halide composition, as perfectly epitomized by the spectrum of the alloy1 (segregated) model associated to the 75:25 I:Br ($MAPbI_{2.25}Br_{0.75}$) composition, which shows a signal centered around 600 ppm, related to pure $PbBr_6$ octahedron. Similar observation holds for the signal of the alloy1 model associated to the 25:75 I:Br ($MAPbI_{0.75}Br_{2.25}$) composition, showing a contribution around 1200 ppm clearly associated to the pure PbI_6 octahedron composing the model. In *Figure 6,c*, we report the isotropic ^{207}Pb chemical shifts calculated in all the pure and mixed halide models investigated here, computed for each PbX_6 composition. The response of each ^{207}Pb nuclei is also clearly dependent upon structural details such as bond lengths and bond angles (see next *Section*), leading therefore to significant dispersion (up to 200 ppm) of the NMR signal for a given octahedron composition. Nevertheless, a clear

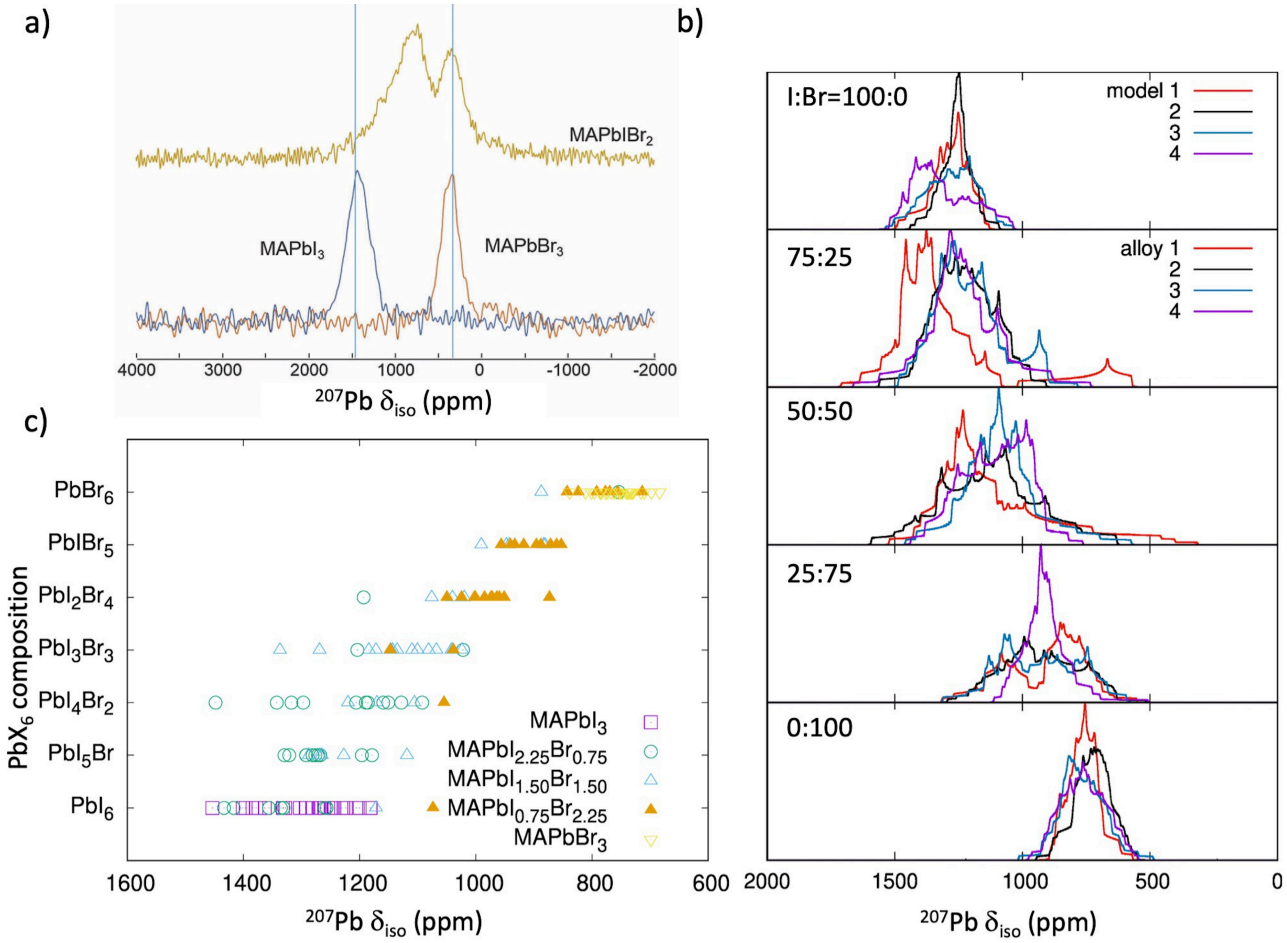

Figure 6. (a) Static ^{207}Pb NMR spectra measured for pure halide $MAPbI_3$ and $MAPbBr_3$ perovskites and for mixed halide perovskite with nominal composition $MAPbIBr_2$; (b) ^{207}Pb static NMR spectra computed for various cubic models of pure phases $MAPbI_3$ and $MAPbBr_3$ perovskites and for mixed halide perovskites with different iodine:bromine ratio. Mixed halide models go from more segregated (alloy1) to more homogeneous (alloy4); c) computed isotropic shift of ^{207}Pb nuclei, as function of the composition of the corresponding PbX_6 octahedron. *Figure 6,a* reproduced with permission from Ref.[12] ©2016 *Royal Society of Chemistry*.

downshift is evident for the ^{207}Pb-NMR chemical shift when passing from pure iodide to pure bromide case. Similar trend in the prediction of the NMR response of ^{207}Pb was reported by *Karmakar et al.* for mixed Cl:Br compounds.[56] Adopting non-periodic DFT simulations including ZORA for the estimate of SOC, the authors found theoretical estimates of the isotropic shift of ^{207}Pb in very good agreement with the experimental datum. The present calculations therefore provide a theoretical support for the use of NMR as characterization tool for halide perovskites, suggesting that the NMR response of ^{207}Pb nuclei can be used to estimate the composition of the individual PbX_6 octahedra within mixed halide perovskite systems. In addition, the present calculations shed light on the actual length-scale probed by NMR, clearly showing that this spectroscopic technique is able to track halide segregation already on the scale of the isolated PbX_6 octahedron.

Detailed Structural Information from NMR Response of ^{207}Pb Nuclei

We conclude this perspective on the potential contribution of atomistic simulations to the interpretation of NMR spectroscopic response, by analyzing in more detail the relationship between ^{207}Pb-NMR computed parameters and the detailed atomic structure of the individual perovskite PbX_6 octahedron. To this aim, we performed additional calculations on pure lead iodide composition. First, we considered an ideal cubic $CsPbI_3$ structure with Pm-3m space group symmetry. In the present model, the only adjustable parameter is represented by the Pb–I bond length and we therefore

evaluated the NMR response of ^{207}Pb nuclei with respect to this, as shown in *Figure 7,a*. Noteworthy, the isotropic part of the chemical shift for ^{207}Pb is underestimated by 1000 ppm, considering Pm-3m symmetry, as compared to the orthorhombic-tetragonal and cubic model structures as in *Figures 5* and *6*.[82,84] It should be noted that CSA is always zero as expected, due to lead atom site symmetry in the Pm-3m space

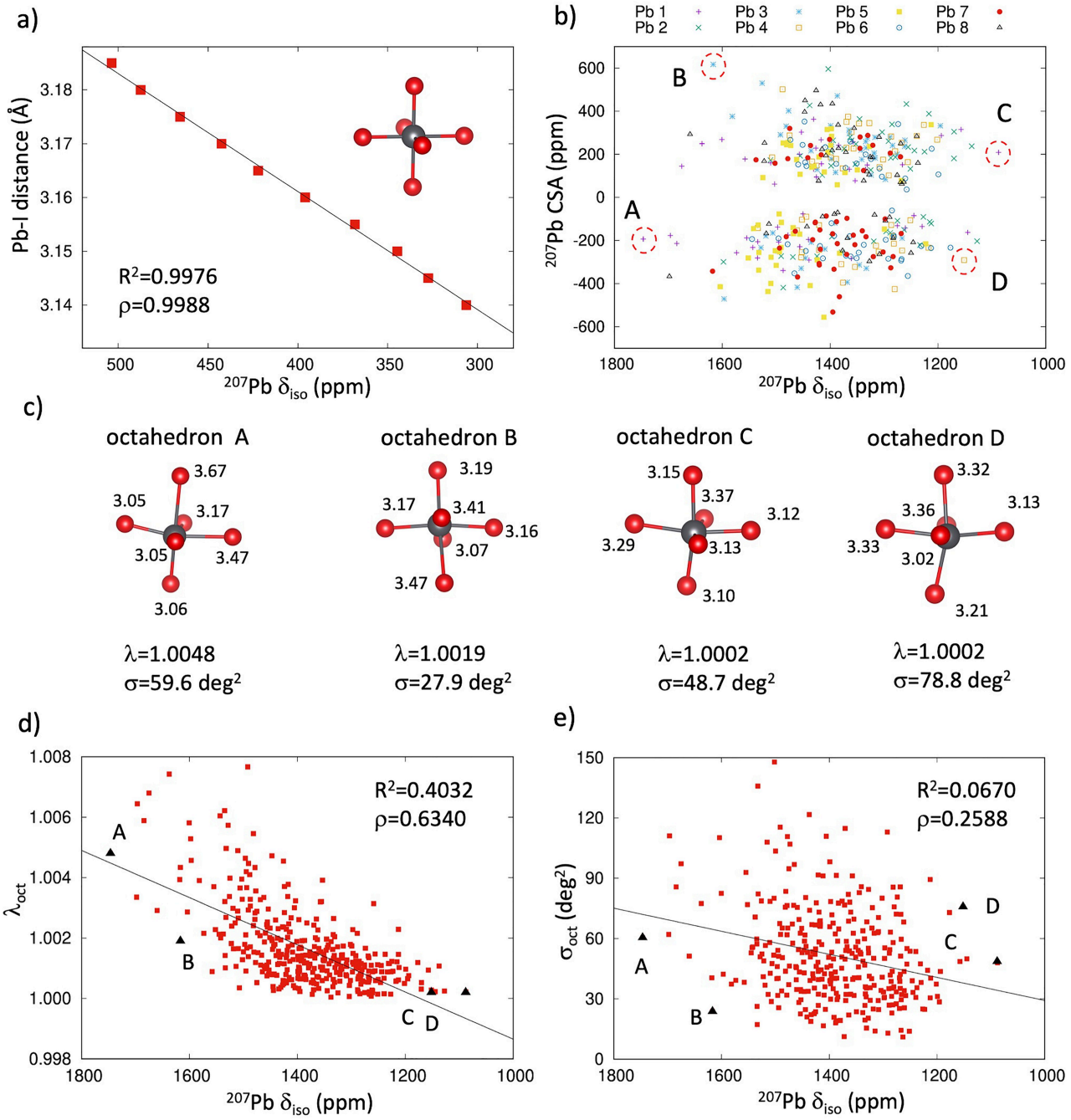

Figure 7. (a) Chemical shift of ^{207}Pb computed for a $CsPbI_3$ perovskite with ideal Pm-3m symmetry, as function of the Pb–I bond length. Linear fitting of the data represented by a black line (corresponding R^2 and *Pearson* ρ coefficient reported); (b) isotropic-shift *vs.* CSA 2D map for ^{207}Pb nuclei, as computed on 50 snapshots extracted along a *Born-Oppenheimer* Molecular Dynamics (BOMD) trajectory; (c) structural analysis of four snapshots selected from the BOMD trajectory. λ_{oct} and σ are the elongation and deformation parameter for PbX_6 octahedra, respectively; (d-e) dependence of the isotropic chemical shift of ^{207}Pb as function of λ_{oct} (d) and σ (e). Linear fitting of the data represented by a black line (corresponding R^2 and *Pearson* ρ coefficient reported).

group. Furthermore, the chemical shift increases with increasing the Pb–I distance, following a trend which is well reproduced by linear fit (R^2 parameter and *Pearson* parameter ρ both very close to unity, as reported in *Figure 7,a*). Notably, such increase can be sizable (on the order of 100 ppm) even for small shrink/elongation (0.02 Å) of the metal-halide bond length compared to the nominal equilibrium value from literature (3.165 Å), as quantified by the slope for the linear fit (4547 ppm/Å).

In order to clarify how the detailed atomistic structure of the perovskite material influences the NMR response of ^{207}Pb atoms, we considered differently distorted $MAPbI_3$ structures as extracted from a short *Born-Oppenheimer* molecular dynamics simulation, considering model cubic 1 of $MAPbI_3$ depicted in *Figure 1*, targeting 300 K temperature. Subsequently, we extracted 50 snapshots along the trajectory, and computed the corresponding NMR response, with results summarized in the isotropic shift-CSA 2D map in *Figure 7,b*. As already pointed out in the literature, NMR response of ^{207}Pb nuclei is spread over large range of isotropic shifts, with CSA ideally influenced by the specific deformation of the PbX_6 octahedron with respect to O_h symmetry. CSA is never close to zero, indicating that the frozen structures as obtained on the fs-timescale from our molecular dynamics present PbI_6 octahedra distorted with respect to ideal Oh symmetry, a fact that has been already pointed out in the literature by molecular dynamics simulations and optical spectroscopic measurements.[10,11,15]

We further dig in potential structure/NMR response correlations, by considering few snapshots from the *Born-Oppenheimer* molecular dynamics trajectory, highlighted in *Figure 7,b*, focusing in particular on lead atoms having either very large or very small isotropic chemical shifts. In light of the very local character of the NMR response, as also pointed out in *Figure 7*, we analyzed the structure of each corresponding PbI_6 octahedron, neglecting structural information related to the organic cations or to second nearest neighbor inorganic atoms. For the four considered octahedra, depicted in *Figure 7,c*, we reported bond lengths, as well as the corresponding octahedral elongation (λ_{oct}) parameter and the octahedral angle variance (σ), widely employed to characterize structural deformations in halide perovskites:[38,85]

$$\lambda_{oct} = \frac{1}{6}\sum_{i=1}^{6}\left(\frac{l_i}{l_0}\right)^2$$

$$\sigma = \frac{1}{11}\sum_{i=1}^{12}(\sigma_i - 90)^2$$

where l_0 is the center-to-vertex distance of a regular polyhedron of the same volume.[86] Large isotropic shifts are associated to octahedra A and B, characterized by at least one very long Pb–I bond (3.5 Å – 3.7 Å, as shown in *Figure 7,c*) compared to the nominal Pb–I average distance, which is reflected by longer λ_{oct} parameter. Small ^{207}Pb isotropic shifts are instead associated to octahedra C and D, characterized by more homogeneous distribution of the Pb–I distances and λ_{oct} value closer to 1. In this sense, it is worth to mention that *Tremblay et al.* already proposed a relationship between the NMR response of lead with respect to the λ_{oct} deformation parameter, for the case of 2D halide perovskites.[38]

To further extend the statistics for this structural analysis, in *Figure 7,d* we report the octahedral elongation λ_{oct} parameter from the snapshots extracted from the molecular dynamics simulation, as function of the corresponding isotropic shift for ^{207}Pb nuclei. Indeed, a general trend is found, for which more elongated octahedra are overall associated to larger chemical shifts. Still corresponding R^2 and *Pearson* ρ coefficients (0.40 and 0.63, respectively) are far from pointing out a univocal correlation between these two quantities, as reflected also by the large dispersion of isotropic shifts (on the order of few hundreds of ppm) for fixed value of the octahedral elongation. In other words, although a trend is found in *Figure 7,d*, it is possible neither to accurately predict the chemical shift of the ^{207}Pb nuclei solely from the elongation parameter λ_{oct}, nor to univocally anticipate the degree of distortion of a PbI_6 octahedron simply from a measured ^{207}Pb isotropic shift. In *Figure 7,e*, we report the same analysis on the basis of the angular distortion parameter σ, but did not find any robust correlation between structural deformation and isotropic shift. Similar result is found for the CSA, which does correlate neither with λ_{oct}, nor with σ (see *Supporting Information*).

Conclusions

Nuclear Magnetic Resonance (NMR) is rapidly becoming a standard tool for the structural characterization of halide perovskite materials. Indeed, either stand alone or in combination with other characterization

tools, this spectroscopic technique has recently demonstrated its strength by unveiling the detailed material structure of various halide perovskite systems, as in the case of 3D mixed halide compounds,[12,29] 3D mixed A-cation systems,[30–34] 2D layered perovskites[37,38] and quantum dots.[39,43] Interpretation of NMR measurements is however inherently complicated by the complexity of the measured NMR features, often arising from the convolution of many structured signals. In this frame, relying on support from theory and simulation would be extremely welcomed. Advanced and accurate modelling approaches based on periodic Density Functional Theory are nowadays available,[44–46] and widely testified by several studies of glassy materials.[48,49] Still, the application of these tools in the field of halide perovskite has been very limited, up to now, at least at the best of the authors knowledge. Here, we report an extensive periodic DFT investigation of the NMR response of lead halide perovskites, with focus on nuclei with spin I = 1/2, and provide several proofs of principle of the possibilities of DFT in supporting NMR structural characterization, for this class of compounds. First, we demonstrate the capability of GIPAW calculations to reproduce experimental NMR signatures of both light (^{1}H and ^{13}C) and heavy nuclei (^{207}Pb) of halide perovskite materials, with overall good accuracy. For the latter, we anticipate that inclusion of Spin-Orbit-Coupling will be mandatory to reach quantitative accuracy for the chemical shielding tensor, considering the important role of SOC on the electronic properties of lead-based halide perovskites.[55,66,67] Nevertheless, calculations neglecting SOC still allow to capture the main trends with respect to chemical composition of the PbX_6 octahedral frame, demonstrating qualitative agreement for the variation of the chemical shift of ^{207}Pb when going from $MAPbI_3$ to $MAPbBr_3$. Second, we confirm NMR as useful tool to characterize mixed halide perovskites systems, providing in particular a detailed local description of the composition of the material, able to suitably probe the lead chemical environment at the individual PbX_6 octahedron level. This aspect is of primary importance for mixed halide perovskite-based devices, as halide mobility and segregation, represents one of the most important challenges for these materials, influencing their stability over time and performances. Third, the present simulations demonstrate the capability of DFT calculations to provide a unique insight in terms of structure-spectroscopic response relationship for the study of halide perovskites. This was done in first place by considering a simplified structural Pm-3m perovskite model. Although one should refrain from considering such simplified model for the accurate prediction of the NMR spectrum of halide perovskites, this clearly demonstrates the dependence of the chemical shift of the ^{207}Pb nuclei with respect to the metal-halide bond length. Structure/spectroscopic response relationships are also demonstrated considering more realistic models, referring to structural descriptors from the literature, namely the octahedral elongation parameter λ_{oct} and the angular distortion σ. Overall, we find a slight correlation between the isotropic shift of ^{207}Pb nuclei and λ_{oct}, with the NMR signal shifting to larger chemical shifts, when increasing the elongation. Our calculations clearly point out that such kind of correlation between the NMR of ^{207}Pb and λ_{oct} is not overall able to univocally assign the structure of the material solely from the NMR measurement but can still be used as qualitative descriptor. Conversely, the isotropic shift of ^{207}Pb nuclei was not found to depend on the angular deformation σ parameter for realistic models. Overall, the present results demonstrate the suitability of periodic DFT-GIPAW calculations to support NMR investigations of halide perovskites, opening new avenues to reach deeper insights into the structural and dynamical features of mixed halide perovskites, hollow and deficient analogues, down to confined systems such as 2D layered perovskites or 1D nanorods, and to 0D systems, featuring non-connected octahedra.[84]

Acknowledgements

This work has been supported by Agence Nationale de la Recherche, project ANR-18-CE05-0026 (MORELESS). Computational investigations were conducted thanks to HPC resources provided by [TGCC/CINES/IDRIS] under the allocation 2020-A0010907682 made by GENCI. *C. Q.* warmly thanks Prof. *Regis Gautier*, Prof. *Nicolas Mercier* and Prof. *Jens Dittmer* for useful discussions. The authors warmly acknowledge the reviewers for their useful comments and suggestions, which overall contributed to the quality of the manuscript.

Author Contribution Statement

C. Q. and *C. K.* conceived the work. *C. Q.* performed the DFT calculations and wrote the manuscript. *E. F.* supervised the DFT calculations and provided techni-

cal support for the data analysis and the representation of the NMR results. All authors contributed to this work, to the discussions, read the manuscript and agree to its contents.

References

[1] D. B. Mitzi, 'Introduction: perovskites', *Chem. Rev.* **2019**, *119*, 3033–3035.

[2] A. K. Jena, A. Kulkarni, T. Miyasaka, 'Halide perovskite photovoltaics: background, status, and future prospects', *Chem. Rev.* **2019**, *119*, 3036–3103.

[3] P. Schulz, K. Cahen, A. Kahn, 'Halide perovskites: is it all about the interfaces?', *Chem. Rev.* **2019**, *119*, 3349–3417.

[4] S. De Wolf, J. Holovsky, S.-J. Moon, P. Löper, B. Nielsen, M. Ledinsky, F.-J. Haug, J.-H. Yum, C. Ballif, 'Organometallic halide perovskites: sharp optical absorption edge and its relation to photovoltaic performance', *J. Phys. Chem. Lett.* **2014**, *5*, 1035–1039.

[5] M. Karakus, S. A. Jensen, F. D'Angelo, D. Turchinovich, M. Bonn, E. Cánovas, 'Phonon–electron scattering limits free charge mobility in methylammonium lead iodide perovskites', *J. Phys. Chem. Lett.* **2015**, *6*, 4991–4996.

[6] C. Wehrenfennig, G. E. Eperon, M. B. Johnston, H. J. Snaith, L. Herz, 'Charge carrier mobilities and lifetimes in organolead trihalide perovskites', *Adv. Mater.* **2014**, *26*, 1584–1589.

[7] https://www.nrel.gov/pv/cell-efficiency.html.

[8] A. Poglitsch, D. Weber, 'Dynamic disorder in methylammoniumtrihalogenoplumbates (II) observed by millimeter-wave spectroscopy', *J. Chem. Phys.* **1987**, *87*, 6373–6378.

[9] C. C. Stoumpos, C. D. Malliakas, M. G. Kanatzidis, 'Semiconducting tin and lead iodide perovskites with organic cations: phase transitions, high mobilities, and near-infrared photoluminescent properties', *Inorg. Chem.* **2013**, *52*, 9019–9038.

[10] J. Even, M. Carignano, C. Katan, 'Molecular disorder and translation/rotation coupling in the plastic crystal phase of hybrid perovskites', *Nanoscale* **2016**, *8*, 6222–6232.

[11] M. Carignano, Y. Saeed, S. Assa Aravind, I. S. Roqan, J. Even, C. Katan, 'A close examination of the structure and dynamics of $HC(NH_2)_2PbI_3$ by MD simulations and group theory', *Phys. Chem. Chem. Phys.* **2016**, *18*, 27109–27118.

[12] C. Roiland, G. Trippé-Allard, K. Jemli, B. Alonso, J.-C. Ameline, R. Gautier, T. Bataille, L. Le Pollès, E. Deleporte, J. Even, C. Katan, 'Multinuclear NMR as a tool for studying local order and dynamics in $CH_3NH_3PbX_3$ (X = Cl, Br, I) hybrid perovskites', *Phys. Chem. Chem. Phys.* **2016**, *18*, 27133–27142.

[13] A. Marronnier, H. Lee, B. Geffroy, J. Even, Y. Bonnassieux, G. Roma, 'Structural instabilities related to highly anharmonic phonons in halide perovskites', *J. Phys. Chem. Lett.* **2017**, *8*, 2659–2665.

[14] C. Quarti, E. Mosconi, F. De Angelis, 'Interplay of orientational order and electronic structure in methylammonium lead iodide: implications for solar cell operation', *Chem. Mater.* **2014**, *26*, 6557–6569.

[15] C. Quarti, E. Mosconi, J. Ball, V. D'Innocenzo, C. Tao, S. Pathak, H. J. Snaith, A. Petrozza, F. De Angelis, 'Structural and optical properties of methylammonium lead iodide across the tetragonal to cubic phase transition: implications for perovskite solar cells', *Energy Environ. Sci.* **2016**, *9*, 155–163.

[16] M. Abdi-Jalebi, Z. Andaji-Garmaroudi, S. Cacovich, C. Stavrakas, B. Philippe, J. M. Richter, M. Alsari, E. P. Booker, E. M. Hutter, A. J. Pearson, S. Lilliu, T. J. Savenije, H. Rensmo, G. Divitini, C. Ducati, R. H. Friend, S. D. Stranks, 'Maximizing and stabilizing luminescence from halide perovskites with potassium passivation', *Nature* **2018**, *555*, 497–501.

[17] G. E. Eperon, T. Leijtens, K. A. Bush, R. Prasanna, T. Green, J. T.-W. Wang, D. P. McMeekin, G. Volonakis, R. L. Milot, R. May, A. Palmstrom, D. J. Slotcavage, R. A. Belisle, J. B. Patel, E. S. Parrott, R. J. Sutton, W. Ma, F. Moghadam, B. Conings, A. Babayigit, H.-G. Boyen, S. Bent, F. Giustino, L. M. Herz, M. B. Johnston, M. D. McGehee, H. J. Snaith, 'Perovskite-perovskite tandem photovoltaics with optimized band gaps', *Science* **2016**, *354*, 861–865.

[18] W. Ke, C. C. Stoumpos, M. Zhu, L. Mao, I. Spanopoulos, J. Liu, O. Y. Kontsevoi, M. Chen, D. Sarma, Y. Zhang, M. R. Wasielewski, M. G. Kanatzidis, 'Enhanced photovoltaic performance and stability with a new type of hollow 3D perovskite {en}$FASnI_3$', *Sci. Adv.* **2017**, *3*, e1701293.

[19] A. Leblanc, N. Mercier, M. Allain, J. Dittmer, V. Fernandez, T. Pauporté, 'Lead- and iodide-deficient $(CH_3NH_3)PbI_3$ (*d*-MAPI): the bridge between 2D and 3D hybrid perovskites', *Angew. Chem. Int. Ed.* **2017**, *56*, 16067–16072.

[20] S. Plesko, R. Kind, J. Roos, 'Structural phase transitions in $CsPbCl_3$ and $RbCdCl_3$', *J. Phys. Soc. Jpn.* **1978**, *45*, 553–557.

[21] S. Sharma, N. Weiden, A. Weiss, '^{207}Pb and ^{205}Tl NMR on perovskite type crystals $APbX_3$ (A=Cs, Tl, X=Br, I)', *Z. Naturforsch., A* **1987**, *42*, 1313–1320.

[22] S. Sharma, N. Weiden, A. Weiss, 'Phase transitions in $CsSnCl_3$ and $CsPbBr_3$. An NMR and NQR study', *Z. Naturforsch. A* **1991**, *46*, 329–336.

[23] R. E. Wasylishen, O. Knop, J. B. Macdonald, 'Cation rotation in methylammonium lead halides', *Solid State Commun.* **1985**, *56*, 581–582.

[24] O. Knop, R. E. Wasylishen, M. A. White, T. S. Cameron, M. J. M. Van Oort, 'Alkylammonium lead halides. Part 2. $CH_3NH_3PbX_3$(X=Cl, Br, I) perovskites: cuboctahedral halide cages with isotropic cation reorientation', *Can. J. Chem.* **1990**, *68*, 412–422.

[25] M. M. Lee, J. Teuscher, T. Miyasaka, T. N. Murakami, H. J. Snaith, 'Efficient hybrid solar cells based on meso-superstructured organometal halide perovskites', *Science* **2012**, *338*, 643–647.

[26] H.-S. Kim, C.-R. Lee, J.-H. Im, K.-B. Lee, T. Moehl, A. Marchioro, S.-J. Moon, R. Humphry-Baker, J.-H. Yum, J. E. Moser, M. Grätzel, N.-G. Park, 'Lead iodide perovskite sensitized all-solid-state submicron thin film mesoscopic solar cell with efficiency exceeding 9%', *Sci. Rep.* **2012**, *2*, 591.

[27] L. Etgar, P. Gao, Z. Xue, Q. Peng, A. K. Chandiran, B. Liu, M. K. Nazeeruddin, M. Grätzel, 'Mesoscopic $CH_3NH_3PbI_3$/TiO_2 heterojunction solar cells', *J. Am. Chem. Soc.* **2012**, *134*, 17396–17399.

[28] T. Baikie, N. S. Barrow, Y. Fang, P. J. Keenan, P. R. Slater, R. O. Piltz, M. Gutmann, S. Mhaisalkar, T. J. White, 'A

combined single crystal neutron/X-ray diffraction and solid-state nuclear magnetic resonance study of the hybrid perovskites $CH_3NH_3PbX_3$ (X=I, Br and C', *J. Mater. Chem. A* **2013**, *3*, 9298–9307.

[29] B. A. Rosales, L. Men, S. Cady, M. P. Hanrahan, A. J. Rossini, J. Vela, 'Persistent dopants and phase segregation in organolead mixed-halide perovskites', *Chem. Mater.* **2016**, *28*, 6848–6859.

[30] D. Kubicki, D. Prochowicz, A. Hofstetter, P. Péchy, S. M. Zakeeruddin, M. Grätzel, L. Emsley, 'Cation dynamics in mixed-cation $(MA)_x(FA)_{1-x}PbI_3$ hybrid perovskites from solid-state NMR', *J. Am. Chem. Soc.* **2017**, *139*, 10055–10061.

[31] D. J. Kubicki, D. Prochowicz, A. Hofstetter, S. M. Zakeeruddin, M. Grätzel, L. Emsley, 'Phase segregation in Cs-, Rb- and K-doped mixed-cation $(MA)_x(FA)_{1-x}PbI_3$ hybrid perovskites from solid-state NMR', *J. Am. Chem. Soc.* **2017**, *139*, 14173–14180.

[32] L. Hong, J. Milić, P. Ahlawat, M. Mladenović, D. J. Kubicki, F. Jahanabkhshi, D. Ren, M. Gélvez-Rueda, M. A. Ruiz-Preciado, A. Ummadisingu, Y. Liu, C. Tian, L. Pan, S. M. Zakeeruddin, A. Hagfeldt, F. C. Grozema, U. Rothlisberger, L. Emsley, H. Han, M. Grätzel, 'Guanine-stabilized formamidinium lead iodide perovskites', *Angew. Chem. Int. Ed.* **2020**, *59*, 4691–4697.

[33] A. Boziki, D. J. Kubicki, A. Mishra, S. Meloni, L. Emsley, M. Grätzel, U. Rothlisberger, 'Atomistic origins of the limited phase stability of Cs^+-rich $FA_xCs_{(1-x)}PbI_3$ mixtures', *Chem. Mater.* **2020**, *32*, 2605–2614.

[34] W. Xiang, Z. Wang, D. J. Kubicki, X. Wang, W. Tress, J. Luo, J. Zhang, A. Hofstetter, L. Zhang, L. Emsley, M. Grätzel, A. Hagfeldt, 'Ba-induced phase segregation and band gap reduction in mixed-halide inorganic perovskite solar cells', *Nat. Commun.* **2019**, *10*, 4686.

[35] A. Senocrate, I. Moudrakovski, T. Acatürk, R. Merkle, G. Y. Kim, U. Starke, M. Grätzel, J. Maier, 'Slow $CH_3NH_3^+$ Diffusion in $CH_3NH_3PbI_3$ under light measured by solid-state NMR and tracer diffusion', *J. Phys. Chem. C* **2018**, *122*, 21803–21806.

[36] A. M. Askar, G. M. Bernard, B. Wiltshire, K. Shankar, V. K. Michaelis, 'Multinuclear magnetic resonance tracking of hydro, thermal, and hydrothermal decomposition of $CH_3NH_3PbI_3$', *J. Phys. Chem. C* **2017**, *121*, 1013–1024.

[37] J. V. Milić, J.-H. Im, D. J. Kubicki, A. Ummadisingu, J.-Y. Seo, Y. Li, M. A. Ruiz-Preciado, M. I. Bar, S. M. Zakeeruddin, L. Emsley, M. Grätzel, 'Supramolecular engineering for formamidinium-based layered 2D perovskite solar cells: structural complexity and dynamics revealed by solid-state NMR spectroscopy', *Adv. Energy Mater.* **2019**, *9*, 1900284.

[38] M.-H. Tremblay, F. Thouin, J. Leisen, J. Bacsa, A. R. S. Kandada, J. M. Hoffman, M. G. Kanatzidis, A. D. Mohite, C. Silva, S. Barlow, S. R. Marder, '$(4NPEA)_2PbI_4$ (4NPEA = 4-Nitrophenylethylammonium): structural, NMR, and optical properties of a 3×3 corrugated 2D hybrid perovskite', *J. Am. Chem. Soc.* **2019**, *141*, 4521–4525.

[39] L. Piveteau, M. Aebli, N. Yazdani, M. Millen, L. Korosec, F. Krieg, B. M. Benin, V. Morad, C. Piveteau, T. Shiroka, A. Comas-Vives, C. Copéret, A. M. Lindenberg, V. Wood, R. Verel, M. V. Kovalenko, 'Bulk and nanocrystalline cesium lead-halide perovskites as seen by halide magnetic resonance', *ACS Cent. Sci.* **2020**, *6*, 1138–1149.

[40] Y. Chen, S. R. Smock, A. H. Flintgruber, F. A. Perras, R. L. Brutchey, A. J. Rossini, 'Surface termination of $CsPbBr_3$ perovskite quantum dots determined by solid-state NMR spectroscopy', *J. Am. Chem. Soc.* **2020**, *142*, 6117–6127.

[41] A. Leblanc, N. Mercier, M. Allain, J. Dittmer, T. Pauporté, V. Fernandez, F. Boucher, M. Kepenekian, C. Katan, 'Enhanced stability and band gap tuning of α-$[HC(NH_2)_2]PbI_3$ hybrid perovskite by large cation integration', *ACS Appl. Mater. Interfaces* **2019**, *11*, 20743–20751.

[42] W. M. J. Franssen, A. P. M. Kentgens, 'Solid–state NMR of hybrid halide perovskites', *Solid State Nucl. Magn. Reson.* **2019**, *100*, 36–44.

[43] L. Piveteau, V. Morad, M. V. Kovalenko, 'Solid-State NMR and NQR spectroscopy of lead-halide perovskite materials', *J. Am. Chem. Soc.* **2020**, *142*, 19413–19437.

[44] C. Bonhomme, C. Gervais, F. Babonneau, C. Coelho, F. Pourpoint, T. Azaïs, S. E. Ashbrook, J. M. Griffin, J. R. Yates, F. Mauri, C. J. Pickard, 'First-principles calculation of NMR parameters using the Gauge Including Projector Augmented Wave method: a chemist's point of view', *Chem. Rev.* **2012**, *112*, 5733–5779.

[45] C. Van de Walle, P. Blöchl, 'First-principles calculations of hyperfine parameters', *Phys. Rev. B* **1993**, *47*, 4244.

[46] C. J. Pickard, F. Mauri, 'All-electron magnetic response with pseudopotentials: NMR chemical shifts', *Phys. Rev. B* **2001**, *63*, 245101.

[47] S. E. Ashbrook, D. McKay, 'Combining solid-state NMR spectroscopy with first-principles calculations-a guide to NMR crystallography', *Chem. Sci.* **2016**, *52*, 7186–7204.

[48] L. Bouëssel du Bourg, C. Roiland, L. Le Pollès, M. Deschamps, C. Boussard-Plédel, B. Bureau, C. J. Pickard, E. Furet, 'Impact of Te on the structure and ^{77}Se NMR spectra of Se-rich Ge–Te–Se glasses: a combined experimental and computational investigation', *Phys. Chem. Chem. Phys.* **2015**, *17*, 29020–29026.

[49] L. Bouëssel Du Bourg, E. Furet, A. Lecomte, L. Le Pollès, S. Kohara, C. J. Benmore, E. Bychkov, D. Le Coq, 'Experimental and theoretical insights into the structure of tellurium chloride glasses', *Inorg. Chem.* **2018**, *57*, 2517–2528.

[50] S. E. Ashbrook, J. M. Griffin, K. E. Johnston, 'Recent advances in solid-state nuclear magnetic resonance spectroscopy', *Annu. Rev. Anal. Chem.* **2018**, *11*, 485–508.

[51] D. J. Kubicki, D. Prochowicz, A. Hofstetter, S. M. Zakeeruddin, M. Grätzel, L. Emsley, 'Phase segregation in potassium-doped lead halide perovskites from ^{39}K Solid-State NMR at 21.1 T', *J. Am. Chem. Soc.* **2018**, *140*, 7232–7238.

[52] D. J. Kubicki, D. Prochowicz, A. Hofstetter, M. Saski, P. Yadav, D. Bi, N. Pellet, J. Lewiński, S. M. Zakeeruddin, M. Grätzel, L. Emsley, 'Formation of stable mixed guanidinium–methylammonium phases with exceptionally long carrier lifetimes for high-efficiency lead iodide-based perovskite photovoltaics', *J. Am. Chem. Soc.* **2018**, *140*, 3345–3351.

[53] D. J. Kubicki, D. Prochowicz, A. Hofstetter, B. J. Walder, L. Emsley, '^{113}Cd Solid-State NMR at 21.1 T reveals the local structure and passivation mechanism of cadmium in hybrid and all-inorganic halide perovskites', *ACS Energy Lett.* **2020**, *5*, 2964–2971.

[54] M. A. Ruiz-Preciado, D. J. Kubicki, A. Hofstetter, L. McGovern, M. H. Futscher, A. Ummadisingu, R. Gershoni-Poranne, S. M. Zakeeruddin, B. Ehrler, L. Emsley, J. V. Milić,

M. Grätzel, 'Supramolecular modulation of hybrid perovskite solar cells via bifunctional halogen bonding revealed by two-dimensional ^{19}F Solid-State NMR Spectroscopy', *J. Am. Chem. Soc.* **2020**, *142*, 1645–1654.
[55] F. Alkan, C. Dybowski, 'Chemical-shift tensors of heavy nuclei in network solids: a DFT/ZORA investigation of ^{207}Pb chemical-shift tensors using the bond-valence method', *Phys. Chem. Chem. Phys.* **2015**, *17*, 25014–25026.
[56] A. Karmakar, A. M. Askar, G. M. Bernard, V. V. Terskikh, M. Ha, S. Patel, K. Shankar, V. K. Michaelis, 'Mechanochemical synthesis of methylammonium lead mixed-halide perovskites: unraveling the solid-solution behavior using Solid-State NMR', *Chem. Mater.* **2018**, *30*, 2309–2321.
[57] J. H. Noh, J.-H. Im, J. H. Heo, T. N. Mandal, S. I. Seok, 'Chemical management for colorful, efficient, and stable inorganic-organic hybrid nanostructured solar cells', *Nano Lett.* **2013**, *13*, 1764–1769.
[58] A. Sadhanala, F. Deschler, T. H. Thomas, S. E. Dutton, K. C. Goedel, F. C. Hanusch, M. L. Lai, U. Steiner, T. Bein, P. Docampo, D. Cahen, R. H. Friend, 'Preparation of single-phase films of $CH_3NH_3Pb(I_{1-x}Br_x)_3$ with sharp optical band edges', *J. Phys. Chem. Lett.* **2014**, *5*, 2501–2505.
[59] N. J. Jeon, J. H. Noh, W. S. Yang, Y. C. Kim, S. Ryu, J. Seo, S. I. Seok, 'Compositional engineering of perovskite materials for high-performance solar cells', *Nature* **2015**, *517*, 476–480.
[60] D. P. McMeekin, G. Sadoughi, W. Rehman, G. E. Eperon, M. Saliba, M. T. Hörantner, A. Haghighirad, N. Sakai, L. Korte, B. Rech, M. B. Johnston, L. M. Herz, H. J. Snaith, 'A mixed-cation lead mixed-halide perovskite absorber for tandem solar cells', *Science* **2020**, *351*, 151–155.
[61] T. Baikie, Y. Fang, J. M. Kadro, M. Schreyer, F. Wei, S. Mhaisalkar, M. Graetzel, T. J. White, 'Synthesis and crystal chemistry of the hybrid perovskite $(CH_3NH_3)PbI_3$ for solid-state sensitised solar cell applications', *J. Mater. Chem. A* **2013**, *1*, 5628–5641.
[62] Y. Kawamura, H. Mashiyama, K. Hasebe, 'Structural study on cubic-tetragonal transition of $CH_3NH_3PbI_3$', *J. Phys. Soc. Jpn.* **2002**, *71*, 1694–1697.
[63] S. J. Clark, M. D. Segall, C. J. Pickard, P. J. Hasnip, M. I. J. Probert, K. Refson, M. C. Payne, 'First principles methods using CASTEP', *Z. Kristallogr.* **2005**, *220*, 567–570.
[64] F. Alkan, C. Dybowski, 'Spin-orbit effects on the ^{125}Te magnetic-shielding tensor: A cluster-based ZORA/DFT investigation', *Solid State Nucl. Magn. Reson.* **2018**, *95*, 6–11.
[65] R. E. Taylor, F. Alkan, D. Koumoulis, M. P. Lake, D. King, C. Dybowski, L.-S. Bouchard, 'A combined NMR and DFT study of narrow gap semiconductors: the case of PbTe', *J. Phys. Chem. C* **2013**, *117*, 8959–8967.
[66] O. Dmitrenko, S. Bai, P. A. Beckmann, S. van Bramer, A. J. Vega, C. Dybowski, 'The relationship between ^{207}Pb NMR chemical shift and solid-state structure in Pb(II) compounds', *J. Phys. Chem. A* **2008**, *112*, 3046–3052.
[67] B. Adrjan, W. Makulski, K. Jackowski, T. B. Demissie, K. Ruud, A. Antušek, M. Jaszuński, 'NMR absolute shielding scale and nuclear magnetic dipole moment of ^{207}Pb', *Phys. Chem. Chem. Phys.* **2016**, *18*, 16483–16490.
[68] C. Gervais, R. Dupree, K. J. Pike, C. Bonhomme, M. Profeta, C. J. Pickard, F. Mauri, 'Combined first-principles computational and experimental multinuclear Solid-State NMR investigation of amino acids', *J. Phys. Chem. A* **2005**, *109*, 6960–6969.
[69] J. D. Hartman, R. A. Kudla, G. M. Day, L. J. Mueller, G. O. J. Beran, 'Benchmark fragment-based ^{1}H, ^{13}C, ^{15}N and ^{17}O chemical shift predictions in molecular crystals', *Phys. Chem. Chem. Phys.* **2016**, *18*, 21686–21709.
[70] H. A. Posch, W. G. Hoover, F. J. Vesely, 'Canonical dynamics of the Nosé oscillator: Stability, order, and chaos', *Phys. Rev. A* **1986**, *33*, 4253–4265.
[71] M. Bak, J. T. Rasmussen, N. C. Nielsen, 'SIMPSON: A general simulation program for solid-state NMR spectroscopy', *J. Magn. Reson.* **2000**, *147*, 296–330.
[72] A. A. Shmyreva, M. Safdari, I. Furó, S. V. Dvinskikh, 'NMR longitudinal relaxation enhancement in metal halides by heteronuclear polarization exchange during magic-angle spinning', *J. Chem. Phys.* **2016**, *144*, 224201.
[73] M. P. Hanrahan, L. Men, B. A. Rosales, J. Vela, A. J. Rossini, 'Sensitivity-enhanced ^{207}Pb Solid-State NMR Spectroscopy for the rapid, non-destructive characterization of organo-lead halide perovskites', *Chem. Mater.* **2018**, *30*, 7005–7015.
[74] D. J. Kubicki, D. Prochowicz, E. Salager, A. Rakhmatullin, C. P. Grey, L. Emsley, S. D. Stranks, 'Local structure and dynamics in methylammonium, formamidinium, and cesium Tin(II) mixed-halide perovskites from ^{119}Sn Solid-State NMR', *J. Am. Chem. Soc.* **2020**, *142*, 7813–7826.
[75] W. T. N. Van Gompel, R. Herckens, G. Reekmans, B. Ruttens, J. D'Haen, P. Adriaensens, L. Lutsen, D. Vanderzande, 'Degradation of the formamidinium cation and the quantification of the formamidinium-methylammonium ratio in lead iodide hybrid perovskites by nuclear magnetic resonance spectroscopy', *J. Phys. Chem. C* **2018**, *122*, 4117–4124.
[76] J. Lee, W. Lee, K. Kang, T. Lee, S. K. Lee, 'Layer-by-layer structural identification of 2D Ruddlesden-Popper hybrid lead iodide perovskites by Solid-State NMR spectroscopy', *Chem. Mater.* **2021**, *33*, 370–377.
[77] J. R. Henrickson, P. J. Bray, 'A phenomenological equation for NMR motional narrowing in solids', *J. Magn. Reson.* **1973**, *9*, 341–357.
[78] J. M. Griffin, S. Wimperis, A. J. Berry, C. J. Pickard, S. E. Ashbrook, 'Solid-State ^{17}O NMR spectroscopy of hydrous magnesium silicates: evidence for proton dynamics', *J. Phys. Chem. C* **2009**, *113*, 465–471.
[79] T. Umebayashi, K. Asai, T. Kondo, A. Nakao, 'Electronic structures of lead iodide based low-dimensional crystals', *Phys. Rev. B* **2003**, *67*, 155405.
[80] J. Even, L. Pedesseau, J.-M. Jancu, C. Katan, 'Importance of spin-orbit coupling in hybrid organic/inorganic perovskites for photovoltaic applications', *J. Phys. Chem. Lett.* **2013**, *4*, 2999–3005.
[81] R. K. Harris, E. D. Becker, S. M. Cabral de Menezes, R. Goodfellow, P. Granger, 'NMR nomenclature: nuclear spin properties and conventions for chemical shifts', *Solid State Nucl. Magn. Reson.* **2002**, *22*, 458–483.
[82] M. Aebli, L. Piveteau, O. Nazarenko, B. M. Benin, F. Krieg, R. Verel, M. V. Kovalenko, 'Lead-halide scalar couplings in ^{207}Pb NMR of $APbX_3$ perovskites (A=Cs, methylammonium, formamidinium; X=Cl, Br, I)', *Sci. Rep.* **2020**, *10*, 8229.
[83] E. Malkin, S. Komorovsky, M. Repisky, T. B. Demissie, K. Ruud, 'The absolute shielding constants of heavy nuclei:

resolving the enigma of the ^{119}Sn absolute shielding', *J. Phys. Chem. Lett.* **2013**, *4*, 459–463.

[84] A. Karmakar, M. S. Dodd, X. Zhang, M. S. Oakley, M. Klobukowski, V. K. Michaelis, 'Mechanochemical synthesis of 0D and 3D cesium lead mixed halide perovskites', *Chem. Commun.* **2019**, *55*, 5079–5082.

[85] K. Robinson, G. V. Gibbs, P. H. Ribbe, 'Quadratic elongation: a quantitative measure of distortion in coordination polyhedra', *Science* **1971**, *172*, 567–570.

[86] D. Cortecchia, S. Neutzner, A. R. Srimath Kandada, E. Mosconi, D. Meggiolaro, F. De Angelis, C. Soci, A. Petrozza, 'Broadband emission in two-dimensional hybrid perovskites: the role of structural deformation', *J. Am. Chem. Soc.* **2017**, *139*, 39–42.

Received December 20, 2020
Accepted March 18, 2021

